Ionics (2024) 30:3157–3169
https://doi.org/10.1007/s11581-024-05509-1

RESEARCH

# Fabricated and improved electrochemical properties of layered lithium-rich Co-free manganese-based $Li_{1.2}Mn_{0.6}Ni_{0.2}O_2$ cathode material for lithium-ion batteries

**Sining Liu[1,2] · Xin Yan[1,2,3] · Xinru Tian[1,2,3] · Sinan Li[1,2,3] · Shao-hua Luo[1,2,3]**

Received: 30 January 2024 / Revised: 15 March 2024 / Accepted: 31 March 2024 / Published online: 9 April 2024


## Abstract

To meet the development needs of high-performance and low-cost lithium-ion batteries, lithium-rich Co-free manganese-based cathode materials have become the primary choice for future power batteries based on the advantages of low cost and improved battery performance. Herein, $Li_{1.2}Mn_{0.6}Ni_{0.2}O_2$ is prepared by the high-temperature solid-state method. The impacts of calcination temperature, holding time, and heating rate on the microstructure and properties of cathode materials are systematically studied via orthogonal experiments. Results revealed that $Li_{1.2}Mn_{0.6}Ni_{0.2}O_2$ prepared by the high-temperature solid-state method at a calcination temperature of 900 °C, holding time of 12 h, and heating rate of 15 °C/min is ideal, with a smaller particle size and uniform particle distribution and a lower agglomeration degree, and the initial discharge specific capacity reaches 148.4 mAh·g$^{-1}$ at 0.1 C. The discharge specific capacity of 102.8 mAh·g$^{-1}$ is still maintained after 100 charge–discharge cycles. Among the various factors, holding time has the greatest influence on the lithium-rich Co-free manganese-based cathode material. The crystallinity, electrochemical properties, and microstructure of the material prepared at 12 h were considerably better than those prepared under other conditions. Test findings show that with a small particle size and uniform distribution, the synthesized cathode material has better rate and cycle performances.

**Keywords** Lithium-ion battery · Cathode · $Li_{1.2}Mn_{0.6}Ni_{0.2}O_2$ · High-temperature solid-state method · Orthogonal test

## Introduction

With the increasing popularity of electronic devices and electric vehicles, higher requirements are placed on lithium-ion batteries (LIBs) concerning long battery life and high capacity [1, 2]. Several studies have focused on identifying a cathode material with high overall performance, such as excellent thermal stability, low cost, high specific capacity, and high operating voltage [3–11]. $xLi_2MnO_3 \cdot (1\text{-}x)LiMO_2$ (M = Ni, Co, and Mn) is one such Li-rich Mn-based cathode material with abundant raw materials and excellent performance (with specific capacity, energy density, and operating voltage reaching 250 mAh·g$^{-1}$, 900 Wh·kg$^{-1}$, and > 4.6 V, respectively) as well as low cost and environmental friendliness [12–18]. Cobalt plays an indispensable role in the cathode materials of current LIBs. However, limited and expensive cobalt resources have hindered its applications in the electronic mobile terminal domain. Therefore, researchers have developed cobalt-free cathode materials that retain the advantages of lithium-rich manganese-based cathode materials. Less usage of cobalt reduces manufacturing cost, which has become a new research hotspot [19–27]. At present, the reported lithium-rich cobalt-free manganese-based cathode materials mainly include nickel–manganese binary lithium-rich materials and materials doped on this basis. Hua et al. [28] synthesized $Li_{1.2}Mn_{0.6}Ni_{0.2}O_2$ with a first discharge specific capacity of up to 293 mAh·g$^{-1}$ at 0.1 C and discharge specific capacity of 171 mAh·g$^{-1}$ at 10 C. Li et al. [29] synthesized a cobalt-free material, $Li_{1.2}Mn_{0.6}Ni_{0.2}O_2$, and doped

✉ Shao-hua Luo
tianyanglsh@163.com

[1] School of Materials Science and Engineering, Northeastern University, Shenyang 110819, People's Republic of China

[2] Key Laboratory of Dielectric, Electrolyte Functional Material Hebei Province, Qinhuangdao, People's Republic of China

[3] School of Resources and Materials, Northeastern University at Qinhuangdao, Qinhuangdao 066004, People's Republic of China

it with Nb; the addition of Nb did not change the morphology and grain size of the material. The as-obtained material, $Li_{1.2}Ni_{0.2}Mn_{0.56}Nb_{0.04}O_2$, had an outstanding electrochemical performance and the first discharge specific capacity of 254 mAh·g$^{-1}$ at 0.1 C; after 100 cycles, the capacity retention rate was 92.3%. Wu et al. [30] synthesized $Li[Li_{0.2}Fe_{0.1}Ni_{0.15}Mn_{0.55}]O_2$ by coating different amounts of $AlPO_4$ using the coprecipitation method. At 5 wt% of $AlPO_4$, the initial discharge specific capacity of the material was 220.4 mAh·g$^{-1}$ at 0.1 C. Related studies have found that lithium-rich cobalt-free manganese-based cathode materials have better discharge specific capacity, cycle stability, and rate performance.

Although cobalt-free cathode materials are environmentally friendly and economical, they have low first-cycle Coulombic efficiency and poor rate and cycle performances and can only be produced on a small scale [31–36]. To address the poor cycle stability and improve the overall performance of such materials, optimal process parameters must be used in the high-temperature solid-state method. Further, to satisfy industrial production requirements and improve the practical application of these materials, low-cost raw materials and streamlined process equipment must be used [37].

Herein, $Li_{1.2}Mn_{0.6}Ni_{0.2}O_2$ is synthesized using the high-temperature solid-state method. Orthogonal experiments were performed to prepare cathode materials with different electrochemical behaviors at different calcination temperatures, holding times, and heating rates. By comparing the samples synthesized under different preparation conditions, $Li_{1.2}Mn_{0.6}Ni_{0.2}O_2$ with the best performance was identified.

## Experimental

### *Preparation of $Li_{1.2}Mn_{0.6}Ni_{0.2}O_2$ cathode material*

For this experiment, the raw materials were bought from Tianjin Komio Chemical Reagent Co., Ltd. and Shanghai Aladdin Biochemical Technology Co., Ltd. Their purity was analytically pure. According to the stoichiometric ratio of $Li_{1.2}Mn_{0.6}Ni_{0.2}O_2$, $Li_2CO_3$, $MnO_2$, and NiO were placed in a ball milling tank (to make up for the loss of $Li_2CO_3$ during high-temperature calcination, $Li_2CO_3$ needs to be excessive by 1 ~ 5%) and then mixed with ball milling at a speed of 200 r/min for 3 h to make it fully mixed, then calcined at high temperature. After that, the sample was naturally cooled to room temperature with the furnace and ground to obtain fine powder particles. The synthesis procedure is shown in Fig. 1.

### Determination of process parameters of the high-temperature solid-state method and orthogonal experiment

To explore the influence of temperature change on the sample within a certain range in an orthogonal experiment, the thermogravimetric analysis of $Li_{1.2}Mn_{0.6}Ni_{0.2}O_2$ after ball milling was carried out, as shown in Fig. 2. Within the temperature range of 0–234 °C, the evaporation of aqueous solution in the material and the loss of crystalline water in the raw material constituted the major influencing factors, with a weight loss rate of 2.4%. As the temperature is greater than 700 °C, the change in mass is not obvious, with a weight


**Fig. 1** Synthesis process of $Li_{1.2}Mn_{0.6}Ni_{0.2}O_2$ cathode material

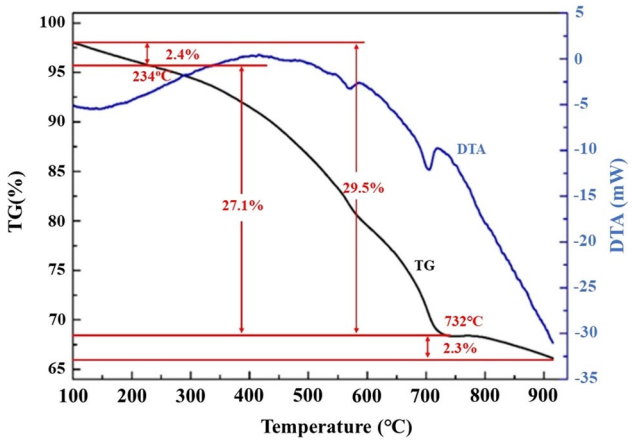


**Fig. 2** TG curves of $Li_{1.2}Mn_{0.6}Ni_{0.2}O_2$

loss rate of 2.3%, indicating that the material has stabilized. According to the thermogravimetric analysis of the material, the temperature range of 700 ~ 900 °C was initially determined as the best calcination temperature.

After determining the range of calcination temperature, this paper carried out a set of orthogonal experiments by controlling the three factors of calcination temperature, holding time, and heating rate, and obtained nine groups of different samples. The specific influencing factors in the experiment are shown in Table 1 below.

## Material characterization

The samples were characterized by X-ray diffraction (XRD; Rigaku, Japan). The diffraction target is Cu Kα ($\lambda = 1.5406$ Å) and the data were acquired at an operating voltage of 40 kV, tube current of 300 mA, and $2\theta = 10°–80°$. The phase of the sample was preliminarily analyzed by the obtained data. The overall morphology of the samples was observed by field emission scanning electron microscopy (FE-SEM; ZEISS SUPRA55, Germany). Thermogravimetric analysis method is used to change the temperature of the sample at the same rate of 10 °C/min and judge the physical and chemical reaction processes of the material according to the change of the sample mass with temperature (TG; HTG-1, China).

**Table 1** The factors and levels of orthogonal experimental

| Level | Calcination temperature (℃) | Holding time (h) | Heating rate (℃/min) |
|---|---|---|---|
| 1 | 700 | 8 | 5 |
| 2 | 800 | 12 | 10 |
| 3 | 900 | 16 | 15 |

## Electrochemical measurements

The mixture was homogeneously mixed in N-methyl pyrrolidone solvent according to the ratio of 80% active substance, 10% acetylene black, and 10% polyvinylidene fluoride, and then coated on aluminum foil to make a working electrode. The rolled aluminum foil was cut into a round sheet with a diameter of about 10 mm under the button cell slicing machine and placed into a vacuum oven, setting the oven temperature to 120 °C, so as to dry. The active material loading mass was around 1.4–2.1 mg. The counter electrode is lithium metal, the electrolyte is 1 mol·$L^{-1}$ $LiPF_6$ solution with a volume ratio of EC:EMC:DMC = 1, and the separator is Celgard 2300. Then, the assembled CR2032 button cell was electrochemically tested.

The charge–discharge and rate performance data were tested by Land CT2001. It is a battery detection system that operates at room temperature with operating voltages from 2.0 to 4.8 V, and EIS (electrochemical impedance spectroscopy) is tested by the Solartron 1260 + 1287 electrochemical impedance analyzers. The frequency range was set from $10^{-1}$ to $10^5$ Hz, and the AC amplitude of all sample tests varied from 5 mV.

# Results and discussion

### *Microstructure analysis of $Li_{1.2}Mn_{0.6}Ni_{0.2}O_2$ orthogonal experimental samples*

The crystal structures of the sintered samples were determined via XRD. Figure 3 shows the XRD patterns of nine $Li_{1.2}Mn_{0.6}Ni_{0.2}O_2$ samples synthesized under different conditions of the orthogonal experiment. The main diffraction

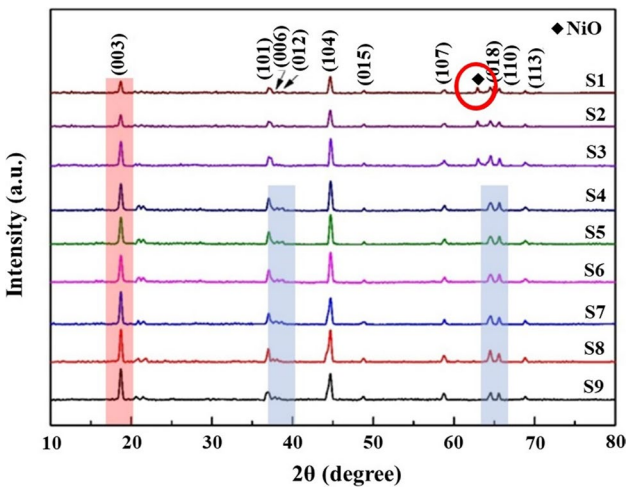


**Fig. 3** XRD patterns of $Li_{1.2}Mn_{0.6}Ni_{0.2}O_2$ synthesized by orthogonal experiment under different conditions

peaks of all samples are consistent with those of the typical layered hexagonal α-$NaFeO_2$, which belongs to the R-3 m space group. The calcination temperature and the intensity of the diffraction peak corresponding to the (003) plane are positively correlated. The impurity phase of NiO also appears in the spectra of S1, S2, and S3, which is related to the dissolution limit of $Ni^{2+}$ in the material. In addition, characteristic peaks of monoclinic $Li_2MnO_3$ are observed at 20°–25°. The diffraction peak intensities differ across all samples, which cause differences in their electrochemical performances. The (006)/(102) and (108)/(110) diffraction peaks of the S4–S9 group cathode materials are split, indicating high crystallinity. Thus, optimal conditions must be selected to ensure crystal growth and enhance performance of $Li_{1.2}Mn_{0.6}Ni_{0.2}O_2$.

Figure 4 illustrates the SEM images of the nine samples synthesized under different conditions. As the sintering temperature increases, the particle distribution and surface of the sample tend to be uniform and flat, respectively. At 900 °C, the particle distribution of the samples is uniform. As the holding time increases, particle agglomeration gradually reduces. Thus, the size and morphology of the sample particles are affected by different preparation process parameters. Thus, an optimal combination of these conditions should exist involving the appropriate selection of holding time and calcination temperature. To verify this assumption, the electrochemical performance of the assembled CR2032 half-cell was tested.

### *Battery performance analysis of $Li_{1.2}Mn_{0.6}Ni_{0.2}O_2$ orthogonal experimental sample*

Electrochemical tests were performed on the nine samples prepared through orthogonal experiments. The first discharge specific capacities of S1–S9 samples are 61.5, 113.2, 145.4, 86.4, 141.1, 118.9, 122.5, 101.4, and 151.3 $mAh{\cdot}g^{-1}$, respectively, as presented in Fig. 5. The discharge specific capacities of S1, S2, and S3 gradually decreased as

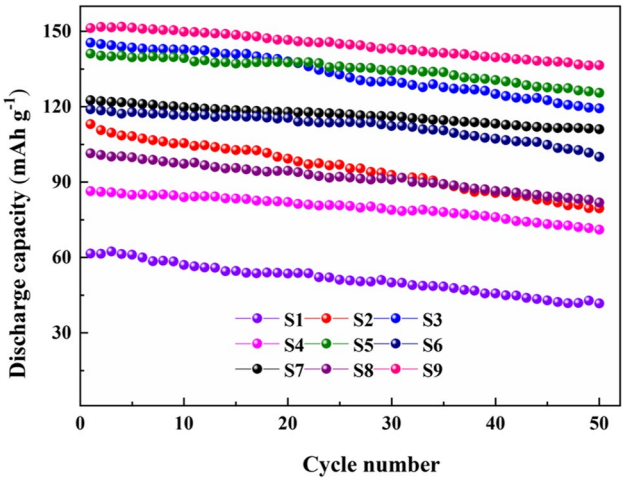


**Fig. 5** Electrochemical properties of nine samples synthesized by orthogonal test

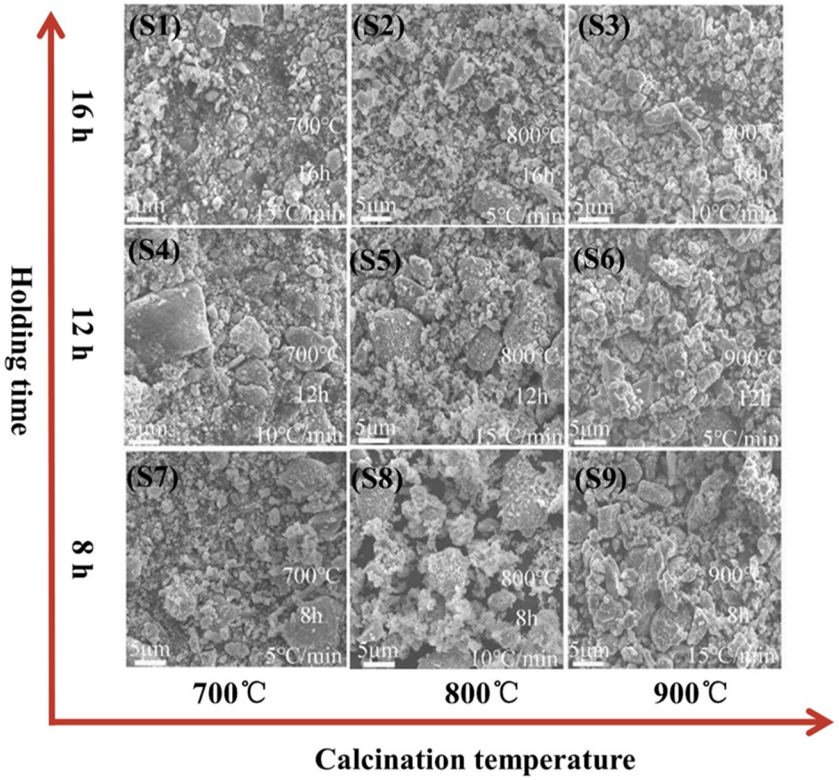


**Fig. 4** SEM image of $Li_{1.2}Mn_{0.6}Ni_{0.2}O_2$ synthesized by orthogonal test under different conditions

the cycle time increased. This demonstrates that 700 °C is not the ideal calcination temperature for the formation of cathode materials. The capacity decay of the remaining samples gradually decreased when the calcination temperature increased, and S9 exhibited a significantly better discharge specific capacity than the other samples.

The range between different levels of each influencing factor is calculated from the results of the orthogonal experiment (Fig. 6). The influence of different process parameters on the discharge specific capacity of $Li_{1.2}Mn_{0.6}Ni_{0.2}O_2$ is in the following order: holding time > heating rate > calcination temperature. Thus, holding time is the most important factor affecting the performance of the material. As the heating rate reaches its maximum value, the influence of holding time and calcination temperature on the microstructure and electrochemical performance of the cathode material is probed by considering the two parameters as a single variable.

### *Effect of calcination holding time on the microstructure of $Li_{1.2}Mn_{0.6}Ni_{0.2}O_2$*

The results show that holding time has the most significant effect on the microstructure and properties of $Li_{1.2}Mn_{0.6}Ni_{0.2}O_2$. Thus, the effects of different holding times, i.e., 8, 10, 12, 16, 20, and 24 h, on the electrochemical properties of $Li_{1.2}Mn_{0.6}Ni_{0.2}O_2$ were studied. The samples prepared at different holding times were tested via XRD; the results are shown in Fig. 7. All six samples show the same major diffraction peaks, except for the C2/m space group in the range of 20°–25°, which corresponds to the spinel structure of $Li_2MnO_3$ (the intensity of the two groups of diffraction peaks in the case of holding times of 8 and 24 h is low and not obvious, indicating that considerably longer or shorter holding times are not conducive to the synthesis

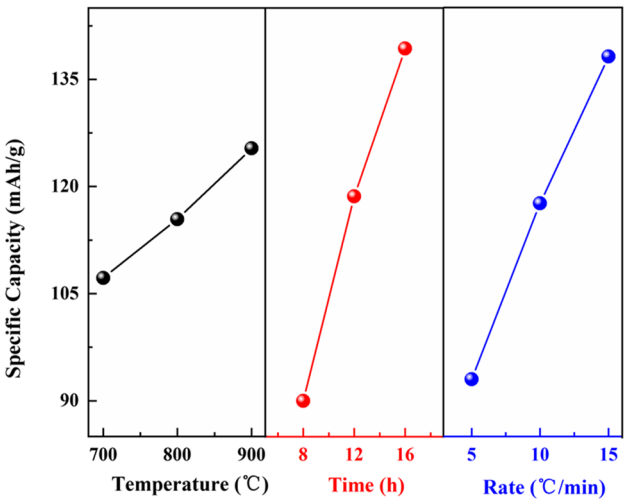


**Fig. 6** Analysis diagram of the results of orthogonal experiment

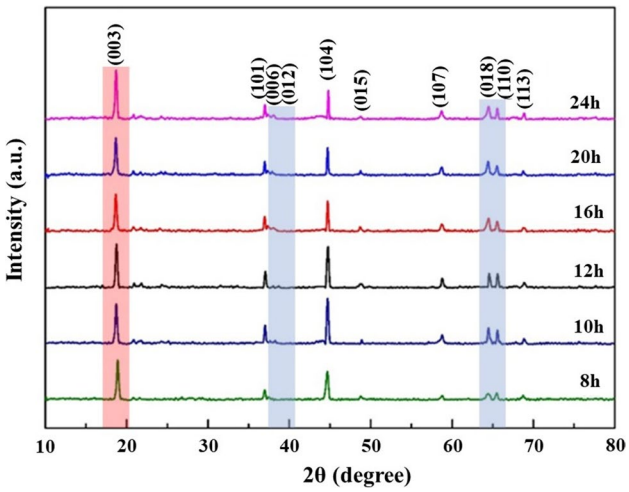


**Fig. 7** XRD patterns of $Li_{1.2}Mn_{0.6}Ni_{0.2}O_2$ samples prepared under different holding times

of the cathode material). The remaining peaks correspond to the α-$NaFeO_2$ layered structure of R-3 m. In addition, the (006)/(012) and (018)/(110) diffraction peaks split, indicating that the layered structure is well characterized in all samples. Except for the aforementioned diffraction peaks, no other impurity peaks appeared in the patterns for all samples. The sample prepared for 12 h exhibited higher diffraction peak intensities, indicating that the material obtained under this condition exhibited the best crystallinity. The crystal size of the samples was calculated using Scheller's formula. The grain size of the sample prepared for 12 h was 49 nm (Table 2); the appropriate grain size was beneficial for enhanced electrochemical performance and mitigating the effects of irreversible capacity.

Figure 8 shows the SEM image of $Li_{1.2}Mn_{0.6}Ni_{0.2}O_2$ fabricated at the holding time of 8, 10, 12, 16, 20, and 24 h. The SEM image demonstrated that with the increase in holding time, the grain size of the samples initially reduces and subsequently increases. After a short holding time of 8 h, the crystal of the material does not grow completely, resulting in large particle sizes, uneven distribution, and poor crystallinity. The samples calcined after holding for 20 h and 24 h have a large damage to the crystal structure of the samples due to the long holding time. Particle agglomeration occurs during the later calcination process. Many particles are heated and bonded together to form an irregular arrangement, which is not conducive to the transmission of $Li^+$ in the crystal, and the electrochemical performance worsens. The sample calcined for 12 h has a small particle size and uniform distribution, and the lithium-ion migration rate is faster, which is beneficial for improving the conductivity of lithium ions. Therefore, 12 h is selected as the best holding time. The particle size distribution diagram indicates that these particles are distributed between 3 and 5 μm. In other

**Table 2** Crystal size of samples with different holding times

| Samples | 8 h | 10 h | 12 h | 16 h | 20 h | 24 h |
|---|---|---|---|---|---|---|
| Crystal size (nm) | 40 | 61 | 49 | 66 | 75 | 27 |

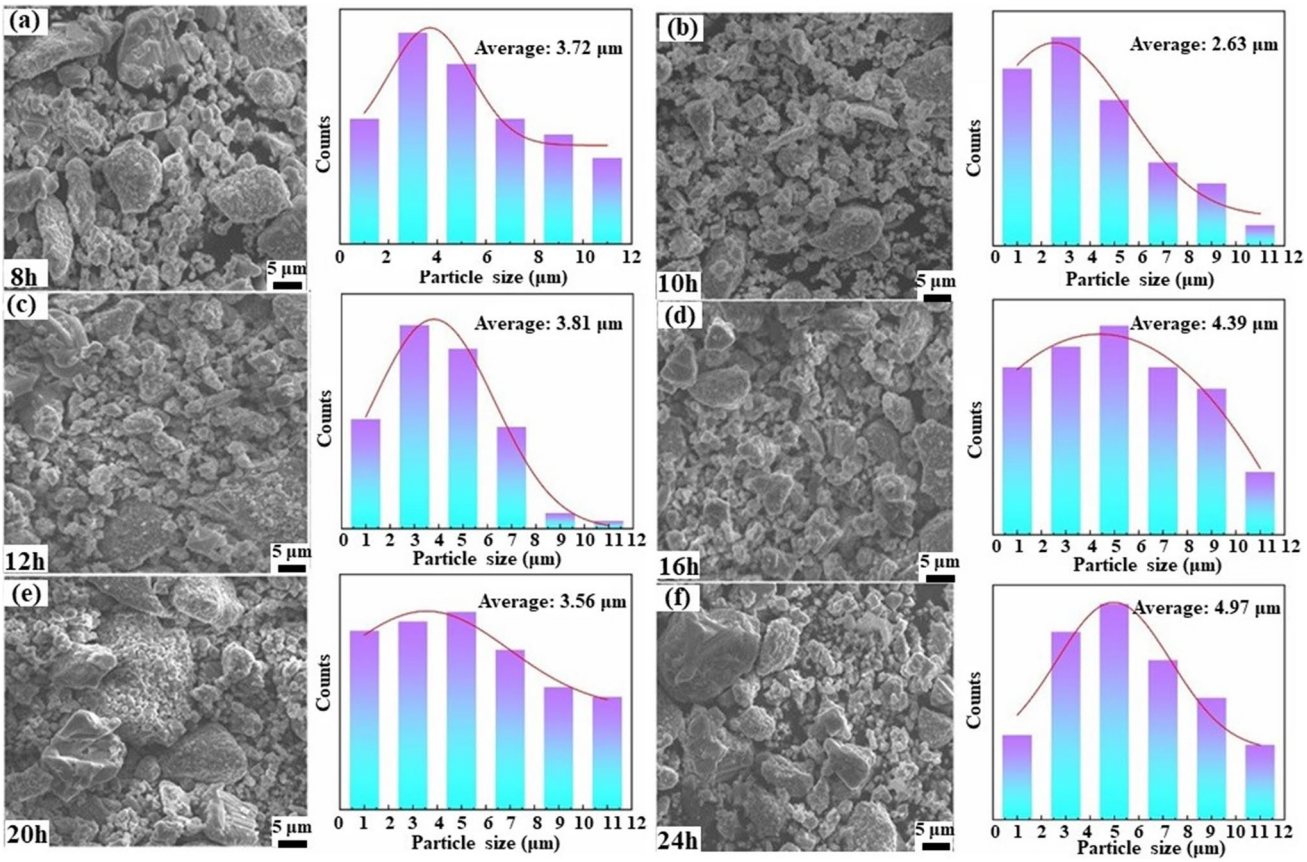


**Fig. 8** SEM images and particle size distribution of $Li_{1.2}Mn_{0.6}Ni_{0.2}O_2$ samples prepared under different holding times: **a** 8 h; **b** 10 h; **c** 12 h; **d** 16 h; **e** 20 h; **f** 24 h

words, many pores are observed in the polygon structure of the $Li_{1.2}Mn_{0.6}Ni_{0.2}O_2$ sample, which can enable rapid electrolyte penetration, accelerate ion diffusion, and improve charge–discharge performance.

### *Effect of calcination time on the electrochemical performance of $Li_{1.2}Mn_{0.6}Ni_{0.2}O_2$*

Figure 9a shows that each sample is charged and discharged 10 times at 0.1–1 C and then returns to the rate performance curve of 0.1 C. At different charge–discharge rates, the discharge specific capacity of the sample prepared for 12 h was considerably higher than that of other samples. At 0.1 C, samples prepared for 12 h had a discharge specific capacity up to 150.8 mAh·g$^{-1}$. At 1 C, the sample exhibits a discharge specific capacity of 85.1 mAh·g$^{-1}$. When returning to 0.1 C again, the sample calcined for 12 h reached 149.1 mAh·g$^{-1}$, and the cathode material synthesized with a holding time of 12 h had better rate performance.

Figure 9b shows that the initial cyclic discharge specific capacity of the sample prepared for 12 h is 149.8 mAh·g$^{-1}$. After 100 cycles, the discharge specific capacity of the sample prepared for 12 h was 105.8 mAh·g$^{-1}$ and the capacity retention rate is 70.6%.

Figure 10a shows the Nyquist plots of the samples prepared for 8, 10, 12, 16, 20, and 24 h with an AC amplitude of 5 mV and a frequency range of 100 kHz–0.01 Hz. There is a marked difference in the low-frequency range. For the low-frequency test, an equivalent circuit was built according to the impedance spectrum, as shown in Fig. 10a, in which $R_s$ is the resistance of the solution, $R_{ct}$ is the resistance to charge transfer, and $W$ is the Warburg impedance. It is observed that the $R_s$ values corresponding to holding times of 8, 10, 12, 16, 20, and 24 h are 10.6, 4.8, 3.9,

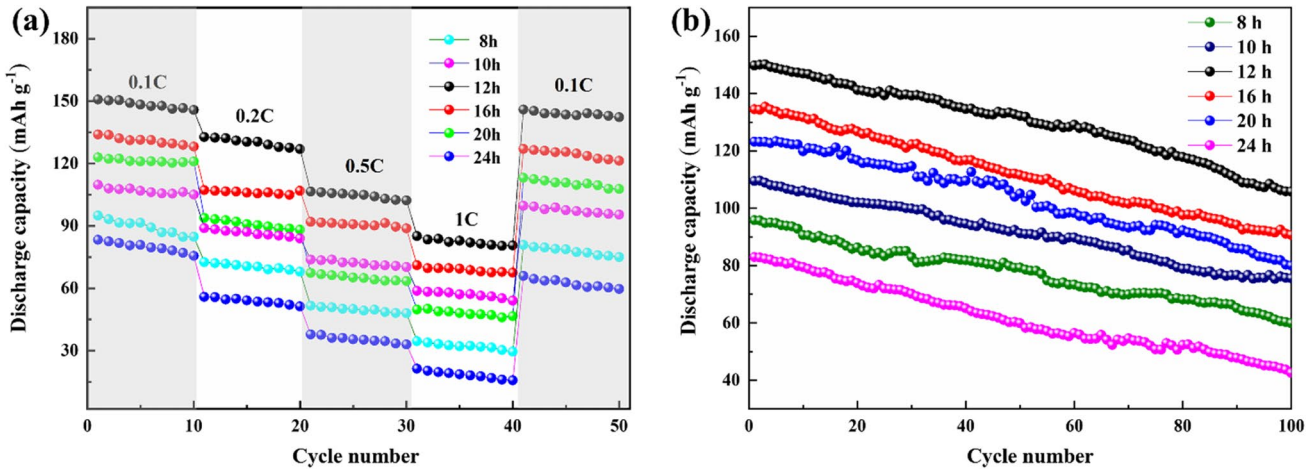


**Fig. 9** Electrochemical characteristic curves of $Li_{1.2}Mn_{0.6}Ni_{0.2}O_2$ synthesized at different holding times: **a** comparison of the rate performance; **b** cycling performance

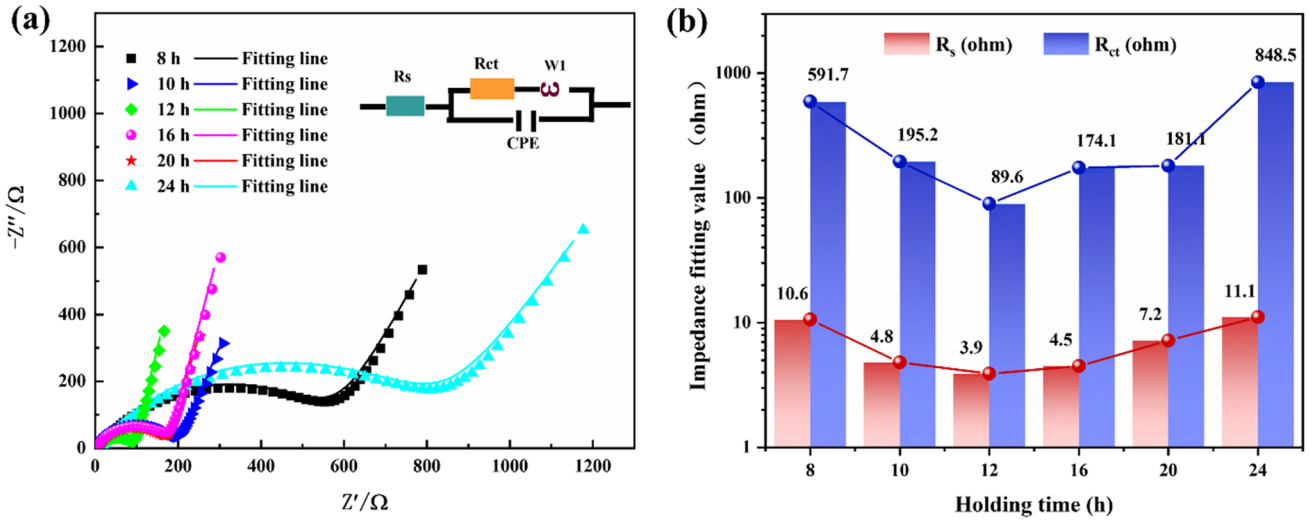


**Fig. 10** **a** The Nyquist plots of $Li_{1.2}Mn_{0.6}Ni_{0.2}O_2$ under different holding times. **b** Electrochemical properties of materials from EIS

4.5, 7.2, and 11.1 Ω, respectively. The $R_{ct}$ values corresponding to holding times of 8, 10, 12, 16, 20, and 24 are 591.7, 195.2, 89.6, 174.1, 181.1, and 848.5 Ω, respectively (Fig. 10b). Thus, the sample prepared at a holding time of 12 h has a low diffusion and charge–discharge resistance. The smaller impedance indicates that an SEI film more stable on the material surface can be formed during charging–discharging cycles, which effectively improves the diffusion rate of $Li^+$ and enhances the rate performance and stability of $Li_{1.2}Mn_{0.6}Ni_{0.2}O_2$.

In order to further explore the effect of holding time on the electrochemical properties of the samples, the diffusion coefficient of $Li^+$ was analyzed by the slope of the low-frequency region in Fig. 10. The diffusion coefficient ($D$) of $Li^+$ can be obtained by the following equation:

$$D_{Li^+} = \frac{R^2T^2}{2A^2n^4F^4C_{Li}^2\sigma^2}$$

$R$ represents the gas constant, which is 8.314 $J{\cdot}mol^{-1}{\cdot}K^{-1}$; $T$ represents the absolute temperature of 298 K; $A$ represents the electrode surface area, which is 0.785 $cm^2$; $n$ denotes the number of electrons; $F$ represents the Faraday constant, and its value is 96,485 $C{\cdot}mol^{-1}$. $C$ represents the concentration of lithium ions in the electrode, and $\sigma$ denotes the coefficient of Warburg (obtained from the slope between $Z_{re}$ and $\omega^{-1/2}$). According to this equation, the diffusion coefficient of lithium ions can be qualitatively estimated by the slope of the straight line in the low-frequency region. The sample prepared under the condition of a holding time of 12 h has the largest linear slope, which indicates that the sample

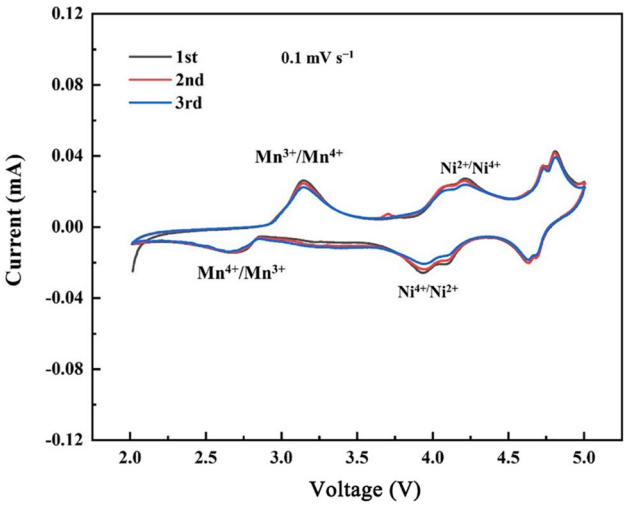


**Fig. 11** CV curves of 12 h sample

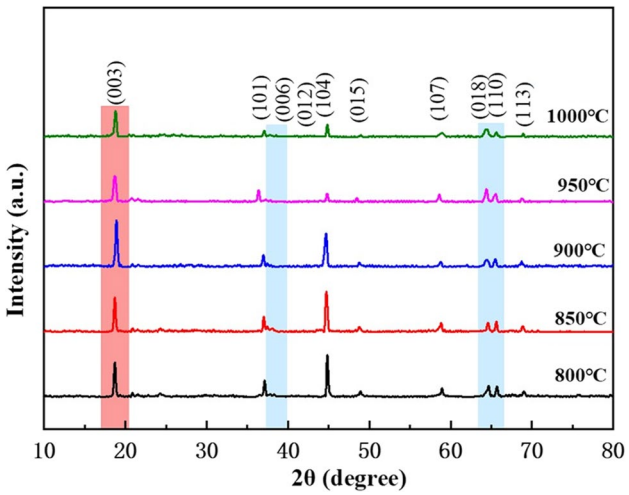


**Fig. 12** XRD patterns of $Li_{1.2}Mn_{0.6}Ni_{0.2}O_2$ samples under different calcination temperatures

under this condition has the largest $Li^+$ diffusion coefficient and thus has the optimal electrochemical performance.

Figure 11 shows the CV curves of the sample prepared for 12 h at a scan rate of 0.1 mV $s^{-1}$, wherein three oxidation peaks are observed. The oxidation peak at ~ 3.1 V corresponds to the reduction of $Mn^{4+}$, which can balance lost oxygen during initial charging. The appearance of the Mn reduction peak in subsequent cycles indicates that Mn participates in the electrochemical reaction. The peak at ~ 4.0 V represents the oxidation of $Ni^{2+}$ to $Ni^{4+}$, which is also accompanied by the removal of Li ions from the lithium layer. The reduction peak at ~ 4.5 V corresponds to $O^{2-}$.

After the optimal holding time was determined to be 12 h, the calcination temperature was subjected to a single factor experiment, and the physical characterization and electrochemical tests were performed at 800, 850, 900, 950, and 1000 °C.

### *Effect of calcination temperature on the microstructure of $Li_{1.2}Mn_{0.6}Ni_{0.2}O_2$*

Figure 12 shows that the crystal diffraction peaks of the samples are similar at different calcination temperatures, which conform to the structural characteristics of the typical layered hexagonal α-$NaFeO_2$ of the R-3 m space group. The five groups of samples exhibit characteristic peaks of $Li_2MnO_3$ belonging to the C-2 m space group between 20° and 25°. These superlattice peaks are due to the arrangement of Li and Mn in the transition metal layer. Moreover, the intensities of the diffraction peaks of (003) and (104) planes first increase and then decrease as the calcination temperature increases, and the diffraction peaks of (006)/(012) also gradually disappear, indicating that the material calcined at 1000 °C has poor crystallinity. Therefore, low temperatures are not conducive to the complete reaction of the material and amorphous materials are easily generated. Moreover, low temperatures hinder the migration of ions and structural reorganization, and the formed material structure has defects and poor crystal form. However, high temperatures are not conducive to the purity improvement of lithium-rich manganese-based cathode materials. Thus, the crystal structure of the sample calcined at 900 °C is relatively optimal. The crystal size of the sample was determined using Scherer's formula; the grain size of the material synthesized at 900 °C was 55 nm (Table 3), which was moderate and consistent with the results shown in Table 2.

Through the refinement of the five groups of samples (Fig. 13), it was found that the *c*/*a* values of all samples were greater than 4.9 (Table 4), indicating that the layered structure of the samples was good. The reason why *c*/*a* increases first and then decrease may be that the increase in activation energy accelerates the migration of ions and promotes the growth of lattice when the calcination temperature increases from 800 to 900 °C. When the temperature is further increased from 900 to 1000 °C, part of the lithium in the lattice is volatilized, so that the lithium site is occupied by other cations, resulting in a decrease in the order of the layered structure.

Next, the effect of calcination temperature on sample morphology was studied in detail. The samples obtained after high-temperature calcination were characterized via SEM. Figure 14 shows that the sample particle size first decreases and then increases as the calcination temperature increases. The particle size distribution of the sample calcined at 800 and 850 °C is not uniform, the surface is rough, small particles are agglomerated, and no obvious regular morphology is observed. As the calcination temperature increases from 950 to 1000 °C, the dispersion of the material becomes poor,

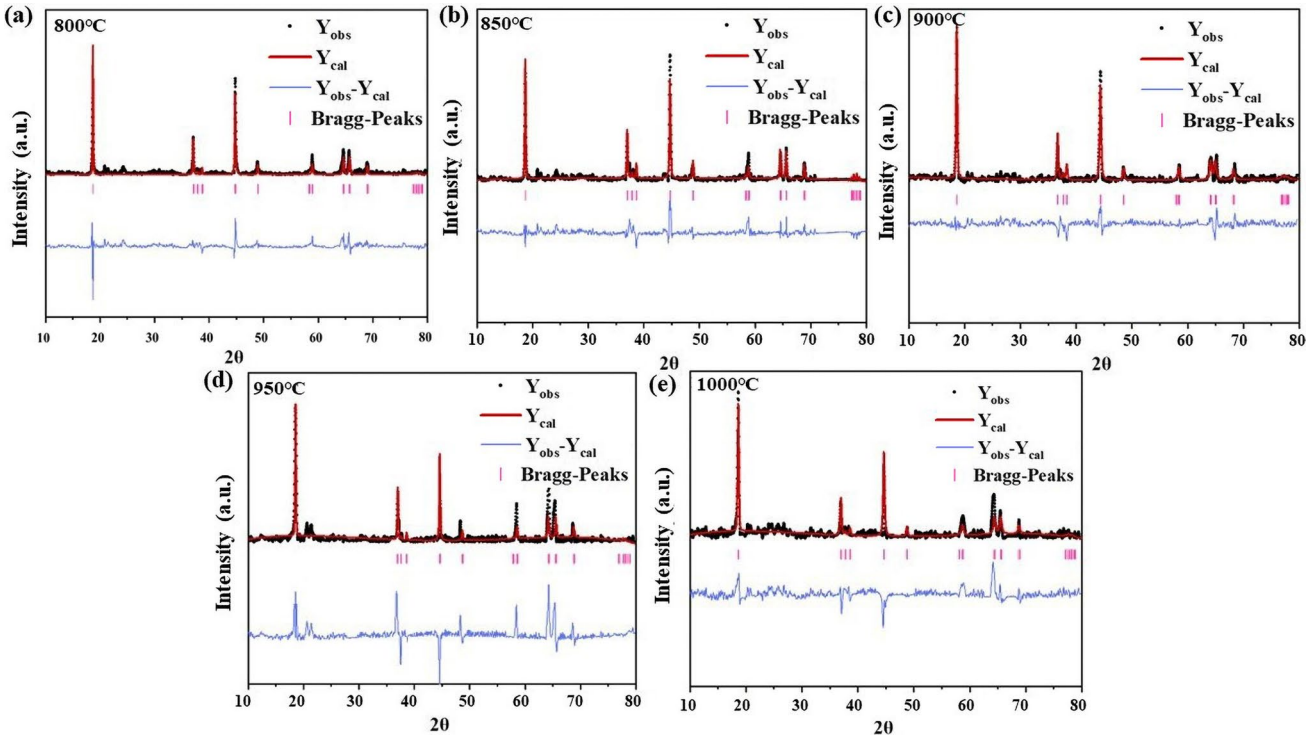


**Fig. 13** Rietveld refinements for $Li_{1.2}Mn_{0.6}Ni_{0.2}O_2$ at different calcination temperatures

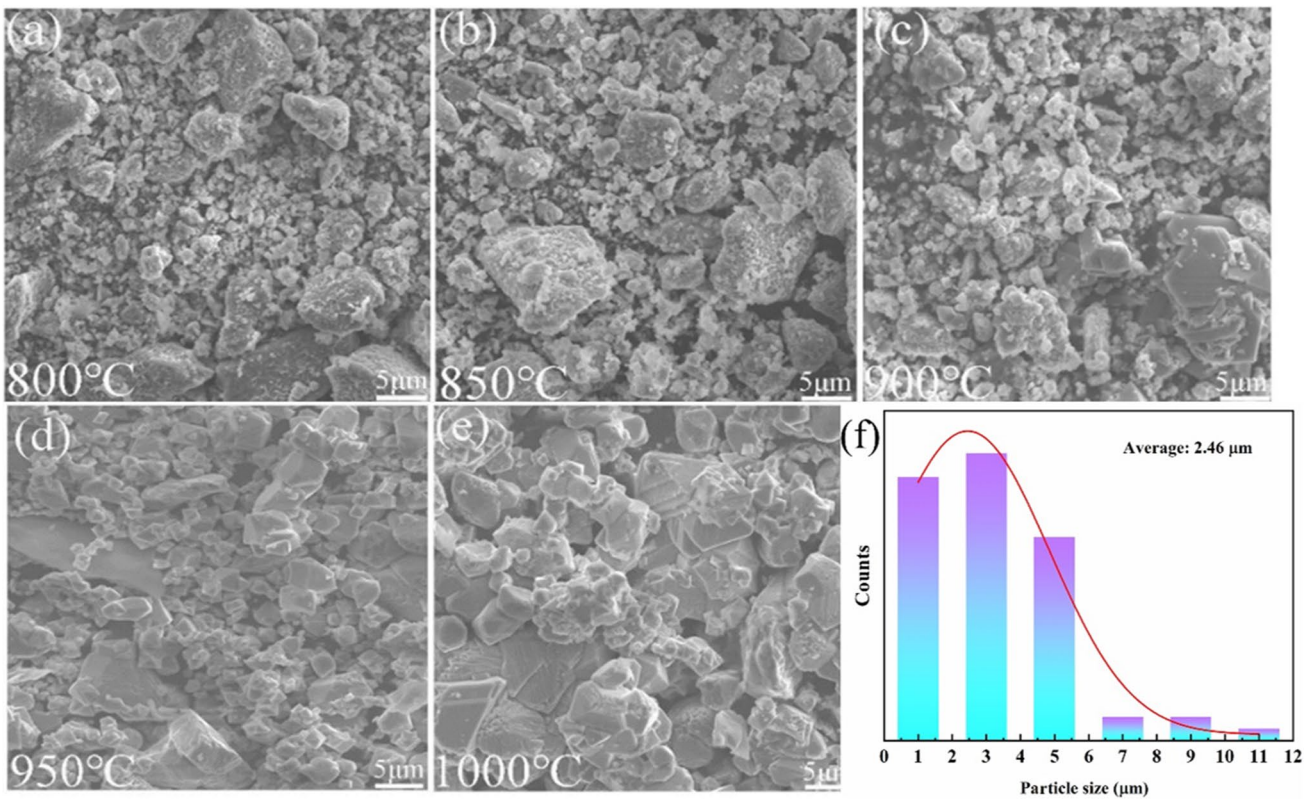


**Fig. 14** SEM pictures of $Li_{1.2}Mn_{0.6}Ni_{0.2}O_2$ samples prepared under different calcination temperatures: **a** 800 ℃; **b** 850 ℃; **c** 900 ℃; **d** 950 ℃; **e** 1000 ℃; **f** particle size distribution of 900 ℃

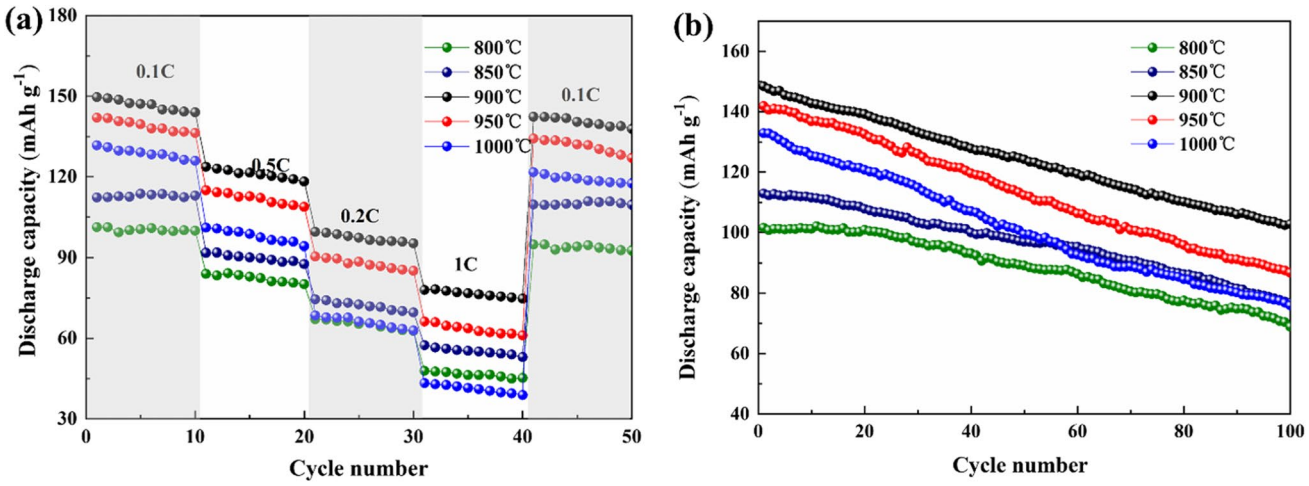


**Fig. 15** Electrochemical characteristic of $Li_{1.2}Mn_{0.6}Ni_{0.2}O_2$ at different calcination temperatures: **a** comparison of the rate performance; **b** cycling performance

leading to the formation of considerably large particles and severe agglomeration, thereby extending the migration distance for $Li^+$ in the material. The resulting smaller contact area between the cathode material and electrolyte is unfavorable for the embedding and detachment of $Li^+$. Thus, the active material in the center of the large particles cannot be fully utilized, thereby decreasing the electrochemical performance of the sample. The particle size is small and particle distribution is uniform for a calcination temperature of 900 °C, which is considered the optimal temperature. In general, smaller particles lead to an increased surface area of the sample, resulting in an increase in the number of particle contact points, thereby increasing the Li-ion dispersion rate and conductivity. Figure 14f shows the grain size distribution of $Li_{1.2}Mn_{0.6}Ni_{0.2}O_2$ synthesized at 900 °C, where the average grain size is 2.46 µm. When the synthesized sample has a relatively minor structure, it can better suit the bulky expanding and contracting of the material during charging–discharging cycles, contributing to the enhancement of its performance concerning Li storage.

### *Effect of calcination temperature on the electrochemical performance of $Li_{1.2}Mn_{0.6}Ni_{0.2}O_2$*

Figure 15a shows the rate performance curves of the five samples. $Li_{1.2}Mn_{0.6}Ni_{0.2}O_2$ calcined at 900 °C has a considerably higher discharge capacity than the other four samples. The calcination temperatures ranged from 800 to 1000 °C

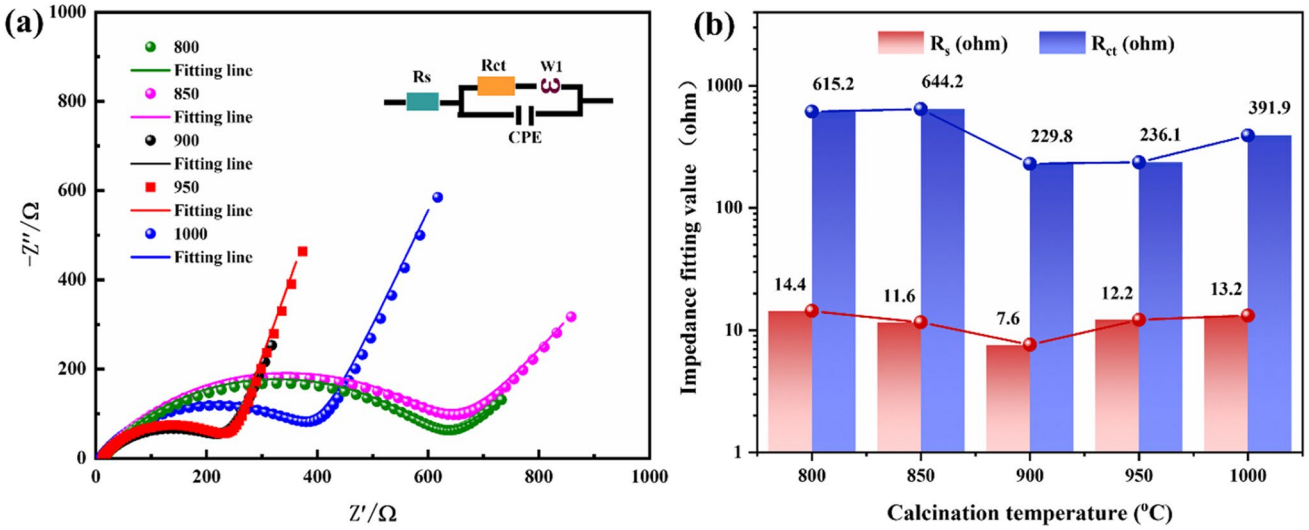


**Fig. 16** **a** The Nyquist plots of $Li_{1.2}Mn_{0.6}Ni_{0.2}O_2$ under different calcination temperatures. **b** Electrochemical properties of materials from EIS.

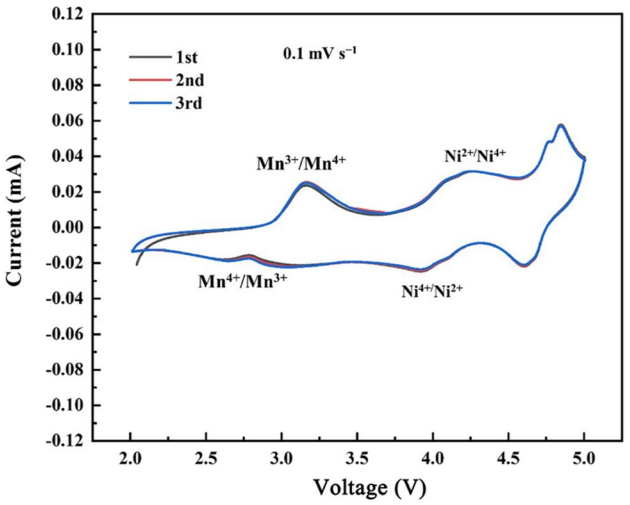


**Fig. 17** CV curves of 900 °C sample

and the initial discharge capacities of the synthesized samples are 101.2, 112.3, 149.6, 142.1, and 131.7 mAh·g$^{-1}$, respectively. At 1 C, the discharge capacities reach 47.8, 57.4, 78.0, 66.2, and 43.3 mAh·g$^{-1}$, respectively. In the aforementioned calcination temperature range, the discharge specific capacity of the cathode material first increases and then decreases, and the sample prepared with a considerably high calcination temperature exhibits a considerably low discharge specific capacity. Combined with the SEM results, it is observed that this is because the primary particles melt and re-grow into a denser product at considerably high calcination temperatures. The resulting poor electrochemical performance of the battery is attributed to the increase of the diffusion distance for $Li^+$ in the unit cell.

Figure 15b demonstrates the discharge capacity curves of the five samples after 100 cycles at 0.1 C. A parallel comparison of calcination temperature makes it not difficult to see that 900 °C was the cyclic stability and capacity retention rate of the sample, which are the most preferred items in each data set. The first discharge specific capacity of the sample was 148.4 mAh·g$^{-1}$, and the capacity retention rate was 69.2% after 100 cycles.

Figure 16a illustrates the electrochemical impedance spectra of the samples synthesized at five calcination temperatures. The $R_s$ values of cathode materials synthesized at 800, 850, 900, 950, and 1000 °C are 14.4, 11.6, 7.6, 12.2, and 13.2 Ω, respectively. The $R_{ct}$ values of cathode materials synthesized at 800, 850, 900, 950, and 1000 °C electrodes are 591.7, 195.2, 89.6, 174.1, 181.1, and 848.5 Ω, respectively (Fig. 16b). S9 has the smallest impedance value, indicating that lithium-ion deintercalation rate is faster and the Li-ion diffusion path is shorter during the charge and discharge processes. The formation rate of spinel structure decelerates and charge transfer is promoted, which exhibits the material with excellent rate and cycle performance. By observing the EIS diagram at different calcination temperatures, it can be found that the straight lines at 900 °C and 950 °C are relatively large. According to the calculation formula for the $Li^+$ diffusion coefficient mentioned above, it can be inferred that the samples prepared at 900 °C and 950 °C have a large lithium-ion diffusion coefficient, and the impedance value of the sample is the smallest at 900 °C. Therefore, when the calcination temperature is 900 °C, the electrochemical performance of the sample is excellent.

Figure 17 shows CV curves of the 900 °C sample at a scan rate of 0.1 mV·s$^{-1}$. In the charge voltage scan, three oxidation peaks can be observed in the sample. The peak of oxidation located at ~ 3.1 V reflects the reduction of $Mn^{4+}$. The peak of oxidation at ~ 4.0 V represents the oxidation of $Ni^{2+}$ to $Ni^{4+}$, which is also accompanied by the detachment of $Li^+$ from the lithium layer. The reduction peak near 4.5 V corresponds to $O^{2-}$, which is in accordance with that obtained in Fig. 10b. Based on these assessments and the studied work, it is clear that the rise in oxidation/reduction capacity is primarily attributable to the redox of Ni and O, with a contribution from the redox of Mn present in the smaller voltage region as well.

In order to make a comparison, the electrochemical properties of the materials prepared in this study under the conditions of holding time of 12 h, calcination temperature of 900 °C, and heating rate of 15 °C/min are summarized in Table 5, along with similar cobalt-free materials reported in the literature. It clearly shows that the materials obtained by optimizing the experimental conditions in this work have a higher discharge capacity.

**Table 3** Crystal size of samples with different calcination temperatures

| Samples | 800 °C | 850 °C | 900 °C | 950 °C | 1000 °C |
|---|---|---|---|---|---|
| Crystal size (nm) | 69 | 60 | 55 | 39 | 26 |

**Table 4** The crystal parameters of the samples at different calcination temperatures

| Crystal data | 800 ℃ | 850 ℃ | 900 ℃ | 950 ℃ | 1000 ℃ |
|---|---|---|---|---|---|
| $a$ (Å) | 2.8403 | 2.8462 | 2.8549 | 2.8461 | 2.8457 |
| $c$ (Å) | 14.2445 | 14.2779 | 14.3427 | 14.2944 | 14.2907 |
| $V$ (Å$^3$) | 99.5191 | 100.1673 | 101.2380 | 100.2760 | 100.2218 |
| $c/a$ | 5.0151 | 5.0165 | 5.0239 | 5.0225 | 5.0219 |
| $R_{wp}$ (%) | 5.16 | 3.43 | 2.94 | 8.15 | 4.18 |
| $R_p$ (%) | 4.83 | 4.62 | 3.36 | 7.10 | 3.76 |

**Table 5** Reported discharge capacity of cobalt-free materials

| Materials | First discharge capacity $mAh{\cdot}g^{-1}$ | Current density | Ref |
|---|---|---|---|
| $Li_{1.1}Ni_{0.35}Mn_{0.55}O_2$ | 135 $mAh{\cdot}g^{-1}$ | 0.1 C | [20, 38–41] |
| $LiNi_{0.5}Mn_{1.5}O_{4-\delta}$ | 109 ~ 122 $mAh{\cdot}g^{-1}$ | 0.05 C | |
| $LiNi_{0.7}Mn_{0.3}O_2$ (H6) | 145 $mAh{\cdot}g^{-1}$ | 0.1 C | |
| $LiNi_{0.5}Mn_{1.5}O_4$ | ~ 132 $mAh{\cdot}g^{-1}$ | 0.1 C | |
| $Li_{1+x}MO_2$ (M = Li, Ni, Mn, Fe) | ~103 $mAh{\cdot}g^{-1}$ | 0.1 C | |
| $Li_{1.2}Mn_{0.6}Ni_{0.2}O_2$ | 148.4 $mAh{\cdot}g^{-1}$ | 0.1 C | This work |

## Conclusion

Herein, a series of lithium-rich Co-free manganese-based $Li_{1.2}Mn_{0.6}Ni_{0.2}O_2$ was prepared by the high-temperature solid-state method. The orthogonal experiment was designed with holding time, heating rate, and calcination temperature as the influencing factors. The results show that the influence of the three factors on the crystal structure, morphology, and electrochemical characteristics of $Li_{1.2}Mn_{0.6}Ni_{0.2}O_2$ is as follows: holding time > heating rate > calcination temperature. The final optimized experimental conditions are a holding time of 12 h, a calcination temperature of 900 °C, and a heating rate of 15 °C/min. Under these experimental conditions, samples have better layered structure, have smaller particle sizes, are well-distributed, and show no apparent agglomeration. At 0.1 C, the first discharge specific capacity is not lower than 148.4 $mAh{\cdot}g^{-1}$, and 102.8 $mAh{\cdot}g^{-1}$ can be maintained after 100 cycles of charge and discharge.

**Author contribution** Sining Liu: conceptualization, methodology, software, investigation, formal analysis, writing—original draft. Shao-hua Luo: conceptualization, funding acquisition, resources, supervision, writing—review and editing, software, validation. Xin Yan: data curation, writing—original draft; supervision. Xinru Tian: visualization, investigation; validation. Sinan Li: data curation, supervision; review.

**Funding** This work was financially supported by the National Natural Science Foundation of China (NSFC) (52274295), the Natural Science Foundation of Hebei Province (E2021501029, E2020501001, A2021501007, E2022501028, E2022501029), the Natural Science Foundation-Steel, the Iron Foundation of Hebei Province (No. E2022501030), the Fundamental Research Funds for the Central Universities (N2323025, N2302016, N2223009, N2223010), and the S&T Program of Hebei (22567627H).

National Natural Science Foundation of China,52274295,Natural Science Foundation of Hebei Province,E2021501029,E2020501001,A2021501007,E2022501028,E2022501029,The Natural Science Foundation-Steel,the Iron Foundation of Hebei Province,No. E2022501030,The Fundamental Research Funds for the Central Universities,N2323025,N2302016,N2223009,N2223010,S&T Program of Hebei,22567627H

**Data availability** No datasets were generated or analyzed during the current study.

## Declarations

**Competing interests** The authors declare no competing interests.

## References

1. Manthiram A (2017) An outlook on lithium ion battery technology. ACS Cent Sci 3:1063–1069. https://doi.org/10.1021/acscentsci.7b00288
2. Zeng X, Zhan C, Lu J, Amine K (2018) Stabilization of a high-capacity and high-power nickel-based cathode for Li-ion batteries. Chem 4:690–704. https://doi.org/10.1016/j.chempr.2017.12.027
3. Bai G, Wei W, Wang B et al (2021) Synthesis and electrochemical properties of high power $Li_{1+x}V_3O_8$ cathode materials for lithium-ion batteries. J Solid State Chem 303:122532. https://doi.org/10.1016/j.jssc.2021.122532
4. Amaraweera THNG, Wijayasinghe A, Mellander B-E, Dissanayake MAKL (2017) Development of $Li(Ni_{1/3}Mn_{1/3}Co_{1/3-x}Na_x)O_2$ cathode materials by synthesizing with glycine nitrate combustion technique for Li-ion rechargeable batteries. Ionics 23:3001–3011. https://doi.org/10.1007/s11581-017-2098-6
5. Shen CH, Liu RS, Gundakaram R et al (2001) Effect of Co doping in $LiMn_2O_4$. J Power Sources 102:21–28. https://doi.org/10.1016/S0378-7753(01)00765-0
6. Xiang Y, Huang M, Jiang Y et al (2021) Ionic liquid assisted hydrothermal synthesis of $0.5Li_2MnO_3{\cdot}0.5LiNi_{0.5}Mn_{0.5}O_2$ for lithium ion batteries. J Alloys Compd 864:158177. https://doi.org/10.1016/j.jallcom.2020.158177
7. Wu L, Liu Y, Zhang D et al (2020) Improved electrochemical performance at high rates of $LiNi_{0.6}Co_{0.2}Mn_{0.2}O_2$ cathode materials by pressure-treatment. J Solid State Chem 289:121487. https://doi.org/10.1016/j.jssc.2020.121487
8. Burkhardt S, Friedrich MS, Eckhardt JK et al (2019) Charge transport in single NCM cathode active material particles for lithium-ion batteries studied under well-defined contact conditions. ACS Energy Lett 4:2117–2123. https://doi.org/10.1021/acsenergylett.9b01579
9. Myung S-T, Maglia F, Park K-J et al (2017) Nickel-rich layered cathode materials for automotive lithium-ion batteries: achievements and perspectives. ACS Energy Lett 2:196–223. https://doi.org/10.1021/acsenergylett.6b00594
10. Yao B, Ding Z, Zhang J et al (2014) Encapsulation of $LiFePO_4$ by in-situ graphitized carbon cage towards enhanced low temperature performance as cathode materials for lithium ion batteries. J Solid State Chem 216:9–12. https://doi.org/10.1016/j.jssc.2014.04.023
11. Liang L, Sun X, Zhang J et al (2019) In situ synthesis of hierarchical core double-shell Ti-doped $LiMnPO_4$@$NaTi_2(PO_4)_3$@C/3D graphene cathode with high-rate capability and long cycle life for

lithium-ion batteries. Adv Energy Mater 9:1802847. https://doi.org/10.1002/aenm.201802847
12. Song C, Feng W, Wang X, Shi Z (2020) Enhanced electrochemical performance of $Li_{1.2}Mn_{0.54}Ni_{0.13}Co_{0.13}O_2$ cathode material with bamboo essential oil. Ionics 26:661–672. https://doi.org/10.1007/s11581-019-03233-9
13. Lee Y, Kim MG, Cho J (2008) Layered Li0.88[$Li_{0.18}Co_{0.33}Mn_{0.49}$]$O_2$ nanowires for fast and high capacity Li-ion storage material. Nano Lett 8:957–961. https://doi.org/10.1021/nl0731466
14. Zhu Y, Zhang N, Zhao L et al (2019) Improving electrochemical performance of lithium-rich cathode material $Li_{1.2}Mn_{0.52}Ni_{0.13}Co_{0.13}W_{0.02}O_2$ coated with $Li_2WO_4$ for lithium ion batteries. J Alloys Compd 811:152023. https://doi.org/10.1016/j.jallcom.2019.152023
15. Oishi M, Yogi C, Watanabe I et al (2015) Direct observation of reversible charge compensation by oxygen ion in Li-rich manganese layered oxide positive electrode material, $Li_{1.16}Ni_{0.15}Co_{0.19}Mn_{0.50}O_2$. J Power Sources 276:89–94. https://doi.org/10.1016/j.jpowsour.2014.11.104
16. Liu H, Tao L, Wang W et al (2019) Effects of raw materials on the electrochemical performance of Na-doped Li-rich cathode materials Li[$Li_{0.2}Ni_{0.2}Mn_{0.6}$]$O_2$. Ionics 25:959–968. https://doi.org/10.1007/s11581-018-2696-y
17. Konishi H, Hirano T, Takamatsu D et al (2018) Electrochemical reaction mechanisms under various charge-discharge operating conditions for $Li_{1.2}Ni_{0.13}Mn_{0.54}Co_{0.13}O_2$ in a lithium-ion battery. J Solid State Chem 262:294–300. https://doi.org/10.1016/j.jssc.2018.03.028
18. Liang L, Li X, Su M et al (2023) Chemomechanically stable small single-crystal Mo-doped $LiNi_{0.6}Co_{0.2}Mn_{0.2}O_2$ cathodes for practical 4.5 V-class pouch-type Li-ion batteries. Angew Chem Int Ed 62:e202216155. https://doi.org/10.1002/anie.202216155
19. Ke W, Jiang Y, Han Y et al (2021) In situ functionally utilize surface residual lithium of Co-free Li-rich layered oxides. Ionics 27:3837–3846. https://doi.org/10.1007/s11581-021-04110-0
20. Ulu Okudur F, Mylavarapu SK, Safari M et al (2022) $LiNi_{0.5}Mn_{1.5}O_{4-\delta}$ (LNMO) as Co-free cathode for lithium ion batteries via solution-gel synthesis: particle size and morphology investigation. J Alloys Compd 892:162175. https://doi.org/10.1016/j.jallcom.2021.162175
21. Hu C, Ma J, Li A et al (2023) Structural reinforcement through high-valence Nb doping to boost the cycling stability of Co-free and Ni-rich $LiNi_{0.9}Mn_{0.1}O_2$ cathode materials. Energy Fuels 37:8005–8013. https://doi.org/10.1021/acs.energyfuels.3c00699
22. Kang S-H, Sun YK, Amine K (2003) Electrochemical and ex situ X-ray study of Li($Li_{0.2}Ni_{0.2}Mn_{0.6}$)$O_2$ cathode material for Li secondary batteries. Electrochem Solid-State Lett 6:A183. https://doi.org/10.1149/1.1594411
23. Yang H, He H, Xia X et al (2023) Enhancing of long cycle and high rate performance of $LiNi_{0.8}Co_{0.15}Al_{0.05}O_2$ by $Li_{1.5}Al_{0.5}Zr_{1.5}(PO_4)_3$ surface coating and $Zr^{4+}$doping. J Solid State Chem 326:124210. https://doi.org/10.1016/j.jssc.2023.124210
24. Wang Y, Yu W, Zhao L et al (2023) $CePO_4$/spinel dual encapsulating on Li-rich Mn-based cathode with novel cycling stability. J Alloys Compd 953:170050. https://doi.org/10.1016/j.jallcom.2023.170050
25. Gu M, Genc A, Belharouak I et al (2013) Nanoscale phase separation, cation ordering, and surface chemistry in pristine $Li_{1.2}Ni_{0.2}Mn_{0.6}O_2$ for Li-ion batteries. Chem Mater 25:2319–2326. https://doi.org/10.1021/cm4009392
26. Abdel-Ghany A, El-Tawil RS, Hashem AM et al (2019) Improved electrochemical performance of $LiNi_{0.5}Mn_{0.5}O_2$ by Li-enrichment and $AlF_3$ coating. Materialia 5:100207. https://doi.org/10.1016/j.mtla.2019.100207
27. Yang P, Li H, Wei X et al (2018) Structure tuned $Li_{1.2}Mn_{0.6}Ni_{0.2}O_2$ with low cation mixing and Ni segregation as high performance cathode materials for Li-ion batteries. Electrochim Acta 271:276–283. https://doi.org/10.1016/j.electacta.2018.01.104
28. Hua W, Chen M, Schwarz B et al (2019) Lithium/oxygen incorporation and microstructural evolution during synthesis of Li-rich layered Li[$Li_{0.2}Ni_{0.2}Mn_{0.6}$]$O_2$ oxides. Adv Energy Mater 9:1803094. https://doi.org/10.1002/aenm.201803094
29. Li X, Xin H, Liu Y et al (2015) Effect of niobium doping on the microstructure and electrochemical properties of lithium-rich layered Li[$Li_{0.2}Ni_{0.2}Mn_{0.6}$]$O_2$ as cathode materials for lithium ion batteries. RSC Adv 5:45351–45358. https://doi.org/10.1039/C5RA01798J
30. Wu F, Zhang X, Zhao T et al (2015) Multifunctional $AlPO_4$ coating for improving electrochemical properties of low-cost Li[$Li_{0.2}Fe_{0.1}Ni_{0.15}Mn_{0.55}$]$O_2$ cathode materials for lithium-ion batteries. ACS Appl Mater Interfaces 7:3773–3781. https://doi.org/10.1021/am508579r
31. Zuo W, Luo M, Liu X et al (2020) Li-rich cathodes for rechargeable Li-based batteries: reaction mechanisms and advanced characterization techniques. Energy Environ Sci 13:4450–4497. https://doi.org/10.1039/D0EE01694B
32. Zhao S, Yan K, Zhang J et al (2021) Reaction mechanisms of layered lithium-rich cathode materials for high-energy lithium-ion batteries. Angew Chem Int Ed 60:2208–2220. https://doi.org/10.1002/anie.202000262
33. Croy JR, Gallagher KG, Balasubramanian M et al (2013) Examining hysteresis in composite $xLi_2MnO_3\cdot(1-x)LiMO_2$ cathode structures. J Phys Chem C 117:6525–6536. https://doi.org/10.1021/jp312658q
34. Mohanty D, Li J, Abraham DP et al (2014) Unraveling the voltage-fade mechanism in high-energy-density lithium-ion batteries: origin of the tetrahedral cations for spinel conversion. Chem Mater 26:6272–6280. https://doi.org/10.1021/cm5031415
35. Liu H, Harris KJ, Jiang M et al (2018) Unraveling the rapid performance decay of layered high-energy cathodes: from nanoscale degradation to drastic bulk evolution. ACS Nano 12:2708–2718. https://doi.org/10.1021/acsnano.7b08945
36. Assat G, Foix D, Delacourt C et al (2017) Fundamental interplay between anionic/cationic redox governing the kinetics and thermodynamics of lithium-rich cathodes. Nat Commun 8:2219. https://doi.org/10.1038/s41467-017-02291-9
37. Uzun D (2015) Boron-doped $Li_{1.2}Mn_{0.6}Ni_{0.2}O_2$ as a cathode active material for lithium ion battery. Solid State Ion 281:73–81. https://doi.org/10.1016/j.ssi.2015.09.008
38. Rajappa Prakasha K, Grins J, Jaworski A et al (2022) Temperature-driven chemical segregation in Co-free Li-rich-layered oxides and its influence on electrochemical performance. Chem Mater 34:3637–3647. https://doi.org/10.1021/acs.chemmater.1c04150
39. Ko S, Lee SC, Lee CW, Im JS (2014) A Co-free layered $LiNi_{0.7}Mn_{0.3}O_2$ cathode material for high-energy and long-life lithium-ion batteries. J Alloys Compd 613:96–101. https://doi.org/10.1016/j.jallcom.2014.06.059
40. Zhao H, Ren Y, Bo X et al (2023) A novel study on COF-based semi-solid electrolyte for spinel $LiNi_{0.5}Mn_{1.5}O_4$ targeting transition metals migration. Scr Mater 223:115101. https://doi.org/10.1016/j.scriptamat.2022.115101
41. Pang WK, Kalluri S, Peterson VK et al (2014) Electrochemistry and structure of the cobalt-free $Li_{1+x}MO_2$ (M = Li, Ni, Mn, Fe) composite cathode. Phys Chem Chem Phys 16:25377–25385. https://doi.org/10.1039/C4CP02864C